Scientific Research Publishing

Advances in Materials Physics and Chemistry, 2026, 16(8), 292-308
https://www.scirp.org/journal/ampc
ISSN Online: 2162-5328
ISSN Print: 2162-531X

Mineralogical Compositions of Mining Resources by Rietveld Simulation of High-Resolution Synchrotron X-Ray Diffraction

Jean Baptiste Zoungrana[1], Brahima Sorgho[1], Lamine Zerbo[1], Gisèle Lecomte Nana[2], Philippe Blanchart[2*]

[1]Laboratory of Molecular Chemistry and Materials (LCMM), Joseph KI-ZERBO University, Ouaga, Burkina Faso
[2]University of Limoges, CNRS, IRCER, UMR 7315, F-87000, Limoges, France
Email: *philippe.blanchart@unilim.fr

How to cite this paper: Zoungrana, J.B., Sorgho, B., Zerbo, L., Lecomte Nana, G. and Blanchart, P. (2026) Mineralogical Compositions of Mining Resources by Rietveld Simulation of High-Resolution Synchrotron X-Ray Diffraction. *Advances in Materials Physics and Chemistry*, **16**, 292-308.
https://doi.org/10.4236/ampc.2026.168017

Received: June 16, 2026
Accepted: August 10, 2026
Published: August 13, 2026

Abstract

The precise characterization of the mineralogical composition of complex mineral resources is a major economic challenge for the mining industry, enabling the optimization of deposit management. This study focuses on the characterization of phosphorites from the Kotchari deposit (Burkina Faso). The methodology combines high-resolution X-ray diffraction (XRD) on ESRF (European Synchrotron Radiation Facility), quantitative Rietveld simulation, and Pair Distribution Function. The results demonstrate that phosphorites are composed of hydroxylapatite, francolite (carbonate-fluorapatite), quartz, and illite. The use of synchrotron radiation offers significantly higher data quality, with increased resolution, a very low noise level, and a very short acquisition time. It enables large series of samples that can be characterized rapidly. The accuracy of Rietveld simulations has been validated by a strong correlation with chemical compositions obtained by X-ray fluorescence (XRF), although minor elements such as iron and fluorine are slightly underestimated due to their distribution within existing mineral structures. It demonstrates that Rietveld simulation of synchrotron data allows for the reliable and rapid determination of the mineralogical composition of complex mineral resources. This method proves to be a powerful tool for ore quality control, acquisition of three-dimensional data, and decision support in large-scale mining operations.

Keywords

Phosphorite, Synchrotron, Rietveld Simulation, X-Ray Diffraction, Pair Distribution Function, Burkina Faso

1. Introduction

The need for innovation in the mining industry and the development of new solutions for material characterization has been the subject of numerous recent publications [1] [2]. Among the main themes explored are advanced X-ray Diffraction (XRD) and Rietveld simulation methodologies [3]. In particular, the Rietveld method enables quantitative mineralogical analysis (QPA) [4]. These publications also explore the development of software and algorithms, including open-source solutions such as Profex, MAUD, EXPO, and Dara, which are able to automate phase identification and quantification [5].

The development of mineral resources is a major economic challenge for which quantitative XRD methods are essential. The characterization of complex ores allows for precise analyses of deposits, enabling three-dimensional mapping of these resources and predicting the behavior of minerals during physicochemical processing [6]-[8].

The Rietveld simulation method offers significant advantages over conventional quantitative X-ray diffraction (XRD) analysis methods, making it an effective tool for mineral powder analysis. This method utilizes the entire diffraction pattern (whole-pattern fitting) [9] and therefore all uses intensity data from the diffraction profile. This allows for the efficient analysis of peak overlaps, which are frequently observed with complex mineral mixtures. Phase quantification is improved by utilizing all reflections, and therefore uncertainty in mass fractions is minimized. Structural disorders, such as that seen in clay minerals, can also be considered. For the detection of minor phases, simulating the entire spectrum allows for the improvement of the quantification of the minority phases. The Rietveld method can also model and correct physical problems related to powder samples, including preferred orientations and instrumental errors, such as sample positioning and zero-point offset.

Beyond simply quantifying phases, the method allows for the extraction of structural and physical parameters. Precise values for lattice parameters and micro-stresses are also obtained, and it is possible to refine atomic positions, site occupancy, and crystallite sizes.

One of the practical advantages of the Rietveld method is that it does not require a calibration curve to quantify crystalline phases with known structures, since the reference quantities are calculated theoretically during the analysis. It saves time and resources by eliminating the need to prepare standard mixtures. By adding an internal standard of known quantities, the method can also determine the total fraction of amorphous phase in a sample.

In this study, we used the BGMN software that determines fundamental parameters (FPA) in its Rietveld simulation method [10]. This is essentially a physical model of the diffraction profile rather than a purely empirical approach. This approach simulates the instrumental contribution to peak shape based on a detailed description of the diffractometer configuration. The simulation uses the physical characteristics of the measuring instrument to calculate the instrumental profiles

as a function of 2θ values. BGMN adds a sample-related function to the peak shape function. This function is modeled by several components, including crystallite size and microstresses.

In summary, BGMN does not simply fit mathematical functions of the observed peaks; it mathematically reconstructs the physical aspects of the X-ray path to ensure that the parameter values (such as grain size or phase fractions) correspond to the material reality of the sample.

BGMN uses a specific programming language, and it is best to use the Profex graphical interface [11] to control the BGMN Rietveld refinement kernel. In particular, Profex allows the identification and quantification of minerals present in a sample and the determination of their mass proportions. It also allows the characterization of minerals with a high structural disorder, such as clays, and enables the calculation of the amorphous phase fraction. Profex includes modules for searching and identifying phases from crystal structure databases (Crystallography Open Database; COD) [12].

It was demonstrated that it is possible to use Profex to obtain the mineralogical composition of rocks. The literature documents the use of Profex on a wide variety of rock formations, including sedimentary rocks and complex ores [13]. Profex is also used for the characterization of widely used industrial products, such as cements and geomaterials [14].

X-ray diffraction was complemented by the characterization of the Pair Distribution Function (PDF) [15], also called $G(r)$. It is the probability of finding pairs of atoms separated by a distance r. $G(r)$, which is obtained experimentally by a Fourier transform of the total diffusion diagram of the powder, according to equation (1).

$$G(r) = 4\pi\left[\rho(r) - \rho_0\right] = \frac{2}{\pi}\int_0^{\infty} Q\left[S(Q) - 1\right]\sin(Q_r)\,\mathrm{d}Q \tag{1}$$

where $\rho(r)$ is the microscopic atomic pair density, ρ_0 is the average atomic density, $S(Q)$ is the total scattering structure function, and Q is the momentum transfer ($Q = 4\pi\sin(\theta)/\lambda$). To obtain a very high-quality PDF diagram, the recorded Q range must be wide. This is why the use of short-wavelength X-rays and high 2θ diffraction angles is necessary. The total scattering data interpreted by the PDF methodology provides quantitative information regarding the phase types and atomic environments [16].

The European Synchrotron Radiation Facility (ESRF) [17] in Grenoble, France, is a powerful light source for characterizing the structure and behavior of matter. Its synchrotron beamlines offer extensive material characterization capabilities, enabling it to address research challenges at every stage of the innovation process.

We used the ID31 beamline, which is dedicated to the study of interfaces and materials processing using high-energy X-rays [18]. It offers a range of high-energy X-ray characterization techniques (75 keV), enabling high-resolution characterizations. The ID31 beamline also allows for measurements by reflectivity (XRR), for wide-angle and small-angle diffraction (WAXS and SAXS), and com-

bined with techniques such as imaging. The beamline's optical design allows for rapid modification of beam properties, such as photon energy, bandwidth, and focus. It also allows for the installation of specific experimental setups.

For this study, we characterized phosphate rocks from a major deposit in eastern Burkina Faso. It is the Kotchari phosphorite deposit [19] that is one of the main mining sites in this geographical area. Kotchari is located 70 km northeast of the town of Arly and approximately 40 km south of the city of Diapaga, as previously mentioned and shown on maps [20]. The deposits have estimated reserves exceeding 100 million tons. The samples studied were taken from three different areas of the local deposits.

As for many phosphorite deposits, they are complex mixtures of different minerals. In general, the mineralogical and chemical composition of phosphate rocks varies considerably depending on their formation process. Our objective is to demonstrate the feasibility of performing efficient quantitative mineralogical analyses of these complex natural mineral mixtures using high-resolution X-ray diffraction. This method is very rapid and allows for the analysis of a large number of rock samples.

Knowing the phosphate mineral content before and during mining operations allows for quality control of the extracted ore. It ensures that the extracted ore meets the required specifications for essential mineral content, while minimizing dilution with waste material. It maximizes the profitability of the mining operation by reducing processing and extraction costs.

2. Experimental

In the mining area, three areas of sampling were identified and samples K31, K32 and K33 were obtained. To ensure if samples have a good spatial representation of the mining areas, we followed common recommendations. Several samples were collected and homogeneously mixed from areas up to 25 meters in size.

The extracted samples were prepared according to several steps: -drying at 80˚C; -crushing to one millimeter of rocks with dimensions on the order of one centimeter; -grinding to 10 μm with an alumina ball mill; -sieving to less than 50 μm.

The characterizations after preparation are as follows: -residual moisture determined by drying at 105˚C for 24 h; -loss of ignition (LOI) determined by heating the powders to 1100˚C in an alumina crucible.

Chemical analyses were performed using an X-ray fluorescence spectrometer (XRF Malvern, PANalytical, Zetium). One g of phosphate powder was dry mixed with 10 g of lithium tetraborate and melted at 1065˚C in a platinum crucible to form transparent glass discs suitable for measurements.

High-resolution synchrotron X-ray diffraction and total scattering measurements were performed on the beamline ID31 at ESRF (European Synchrotron Radiation Facility) [21] [22]. Sample powders were placed inside cylindrical windows held between Kapton discs in a movable sample holder. Each sample was

characterized by transmission (Debye-Sherrer) with an incident X-ray energy of 75.051 keV (λ = 0.16520 Å). The measured intensities were collected using a Pilatus detector. A CdTe detector (1679 × 1475 pixels, 172 × 172 μm^2 each) was positioned so that the incident beam was in a corner of the detector. For high-resolution diffraction experiments, the sample-to-detector distance was 1.5 m and decreased to 0.3 m for total scatter measurements. The background noise from the empty windows was measured and subtracted. The NIST SRM 660b (LaB6) standard was used for geometry calibration with the pyFAI software, followed by image integration, including flat field, geometry, solid angles, and polarization corrections.

Rietveld simulations of high-resolution powder X-ray diffraction (XRD) data use the Profex software. Profex enables phase identification and quantification, as well as structure refinement, and offers numerous functionalities (https://www.profex-xrd.org/). Acquisition specifications are: λ = 0.16520 Å, considered monochromatic; a sample-to-sensor distance of 1.5 m; and detailed detector characteristics. Phase identification was performed using the wide database COD. High-resolution X-ray diffraction (XRPD) data were corrected to remove the very low background noise.

Total diffusion (PDF) data were automatically processed by the PDFgetX3 software for different values of Qmax [23]. The data were then reprocessed using a Lorch modification function to remove termination effects and high-frequency noise contributions. The scattering intensities at small angles were extrapolated from Qmin ~0.3 Å^{-1} to 0, using the concentrations of the chemical elements.

Total scattering spectra were simulated using the PDFGui software (https://www.diffpy.org/) [24]-[26]. It uses a user-friendly and intuitive graphical interface for the PDFfit2 simulation program. This software allows for the complete fitting of the atomic Pair Distribution Function (PDF) profile from X-ray diffraction data and integrates graphical and structural visualization functionalities.

3. Results

The moisture contents of the samples extracted from the Kotchari quarries are 1.30 wt% ± 0.04, 1.33 wt% ± 0.04 and 1.22 wt% ± 0.04 for K31, K32, and K33 samples. The low values indicate that the samples are naturally low in hygroscopicity. This also reveals a low clay mineral content and the absence of nano porosity that could bind water.

X-ray diffraction results of phosphorites K31, K32, and K33 after correction of the background are shown in **Figures 1(a)-(c)**. For these results, experimental values obtained with the ID31 beamline below 0.7˚ 2θ and above 10˚ 2θ were removed for the simulations. To evidence the quality of data from the synchrotron, a comparison of the X-ray diffraction spectra of K31, obtained with the ID31 beamline and with a Brücker D8 (Cu kα), is shown in **Figure 2**, inside a limited distance range. A significant difference in quality is observed, with a reduction in

the background noise, a reduction in peak width, and a better peak separation, particularly for low-intensity peaks, while the measurement time is considerably reduced: 2 h with the Brücker D8 and approximately 3 s with the ESRF ID31 beamline. It enables the characterization of numerous samples in a reduced time and at a lower cost.

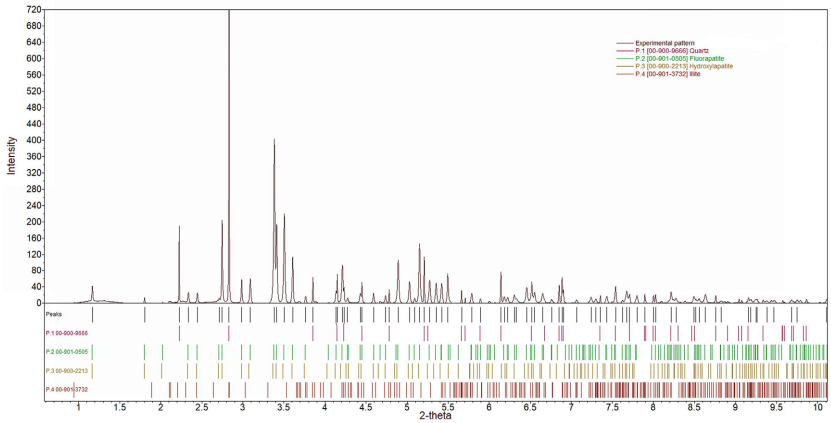

(a)

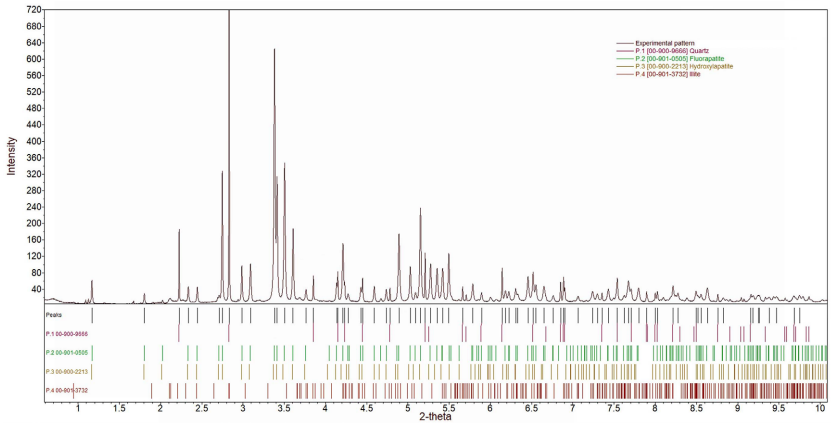

(b)

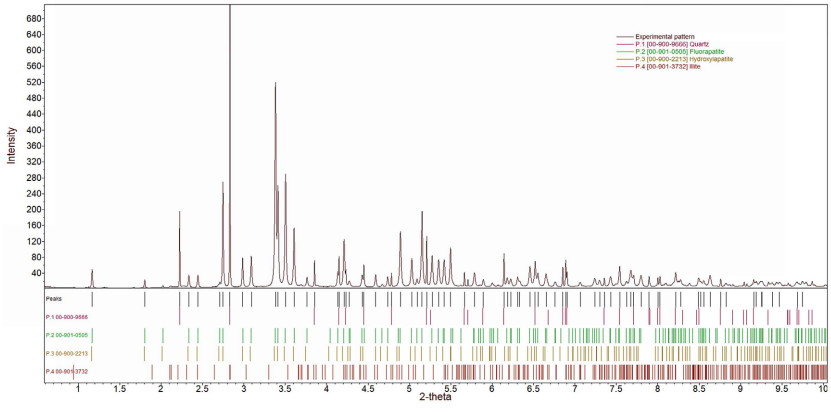

(c)

Figure 1. (a): ID31 beamline DRX pattern of K31 phopsphorite; (b): ID31 beamline DRX pattern of K32 phopsphorite; (c): ID31 beamline DRX pattern of K33 phopsphorite.

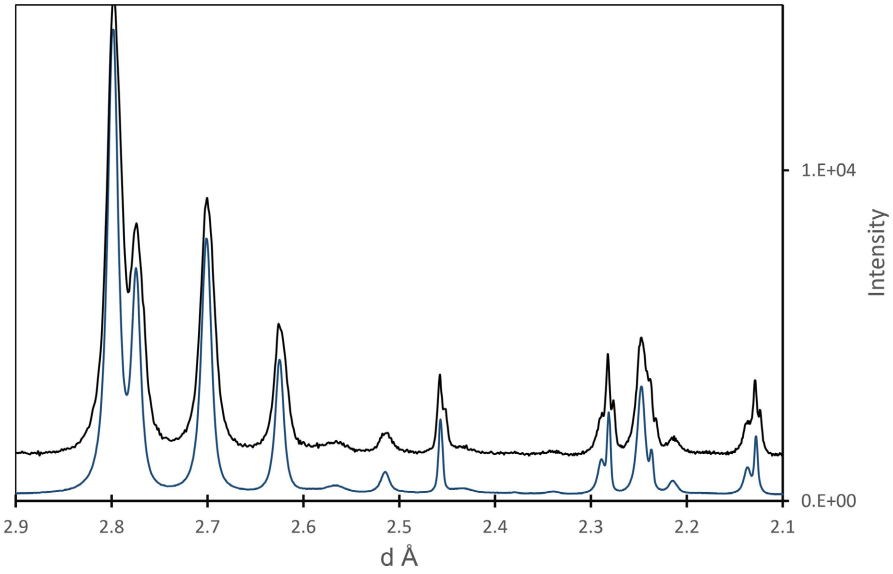

Figure 2. Pattern comparison of K31 phosphorite from ID31 synchrotron beamline (lower pattern), with a 3 s measurement time, and from D8 diffractometer (Brüker), with a 2 h measurement time.

Phase identification was performed using the open-source software QualX [27] and the COD open database. QualX provides a list of the most probable crystalline phases, ranked by the Figure of Merit (FOM) criterion, which considers the positions and amplitudes of the peaks relative to a baseline whose position can be parameterized. The peak positions for each phase are shown in **Figures 1(a)-(c)**, and the data references in the COD database are given in **Table 1**. In **Table 2**, we report the structural models and compositions of mineral phases that are used for calculations. We note that hydroxylapatite and francolite have the same space group that reduces the possibilities to refine the occupancy or substitution for each phase. Consequently, the typical formulas were used for the oxide backcalculation.

Rietveld simulations of X-ray diffraction data were performed using BGMN software and the Profex v.5.0.1 graphical interface. To determine the peak shape, Profex -BGMN uses instrumental characteristics, namely the primary beam, the secondary beam (filtering and beam shaping), the spectral distribution of the X-ray source, and the detector type. The peak profile is also obtained with the contribution of the phases, *i.e.*, the crystallite size and the extent of micro-strains. The instrumental parameters were fixed and remained unchanged during the Rietveld simulations, while the phase contribution was calculated. For baseline calculation, the degree of the polynomial was set to 11. Representative parameter limits for computation were either established in advance in structural models or adjusted to enhance the stability of the refinement and the convergence of the calculated parameters.

Powder X-ray diffraction patterns were simulated between 0.7 and 10˚ 2θ (λ = 0.16520 Å). Plots of simulations are in **Figures 3-5** for K31, K32, and K33 samples. By applying the parameter limits given in the structural models, we calculated the

lattice parameters, phase fractions, and preferred orientations, taking into account microstrains and isotropic broadening of the lines. Non-structural parameters, including the zero-point, sample displacement, and diffraction pattern baseline, were calculated simultaneously. Typical values for the cation occupancy rates defined in the models were used. For all samples, the quality of simulations was from Rwp and Rexp, and is reported in Table 1.

Table 1. Mineralogical composition by Rietveld simulation (wt%). The COD references are CIF files obtained from the Crystallography Open Database (https://crystallography.net/).

	Quartz	Carbonate Fluorapatite	Hydroxylapatite	Illite	Rwp-Rexp
COD reference	9009666	9010505	9002213	9013732	-
K31 (wt%)	25.69	31.30	34.00	9.01	7.76 - 5.75
K32 (wt%)	19.25	33.41	43.02	4.32	7.87 - 6.28
K33 (wt%)	21.00	34.00	38.00	7.00	7.56 - 5.95

Table 2. Structural models and compositions used of mineral phases used in the refinements.

Name	Space group nb.; Hermann Mauguin	Formula
Quartz; cod9009666	152; P3_121	O2_Si
Fluorapatite; cod9010505	176; P6_3/m	C0.078_Ca5_F0.842_O12.402_P2.895
Hydroxylapatite; cod9002213	176; P6_3/m	Ca5_H_O13_P3
Illite; cod9013718	12; C12/m1	Al2_H2_K_O12_Si4

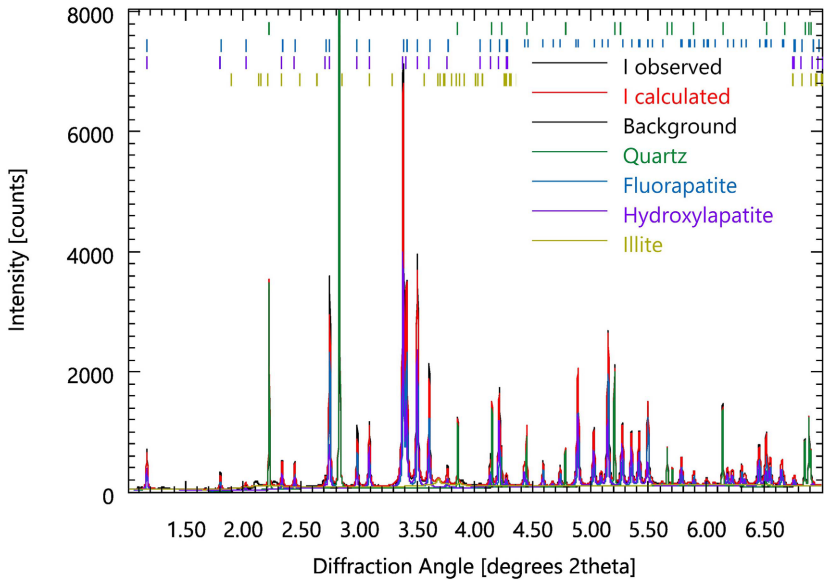

Figure 3. Rietveld simulation of K31 phosphorite, in the range of 0.7˚ - 7˚ 2θ.

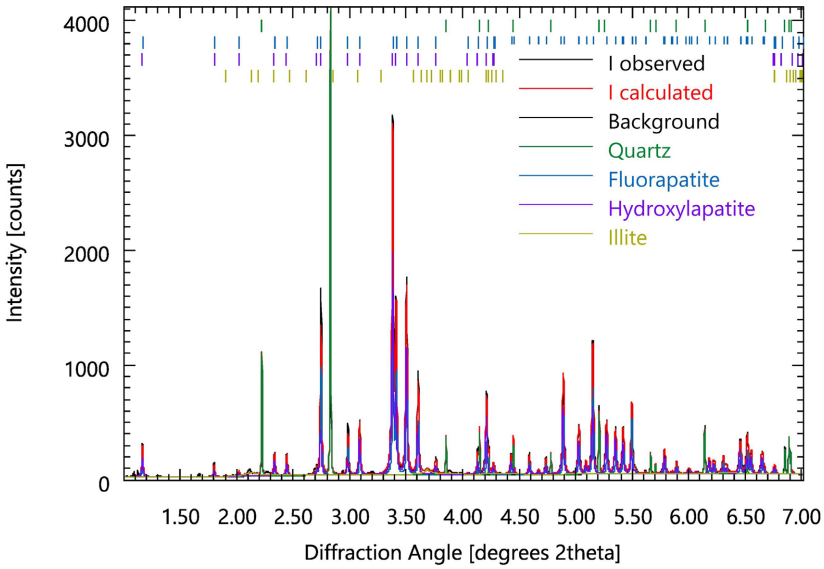

Figure 4. Rietveld simulation of K32 phosphorite, in the range of 0.7˚ - 7˚ 2θ.

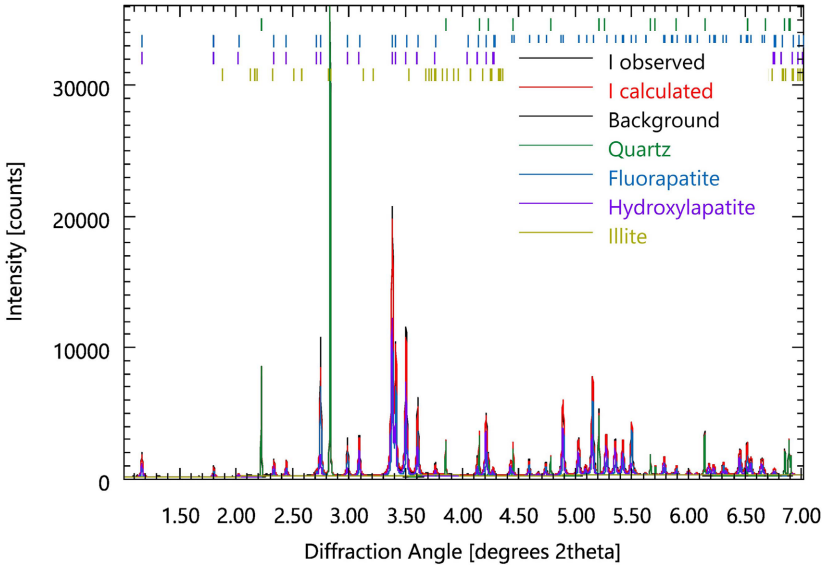

Figure 5. Rietveld simulation of K33 phosphorite, in the range of 0.7˚ - 7˚ 2θ.

Figure 6 shows the experimental pair distribution function (PDF) obtained from synchrotron X-ray diffraction data. The first two peaks correspond to the closest distances for apatite and quartz. It is Si-O at 1.6067 Å and P-O at 1.587 Å in hydroxylapatite, and 1.5324, 1.5388, and 1.5273 Å in francolite. Note that there are a few oscillations preceding and above the Si-O peak, which are termination undulations due to the FFT calculation method, and resulting from the relatively high Q range (25 $Å^{-1}$), as well as instrumental contributions. To improve data quality, we attempted to apply various error-minimizing procedures, such as smoothing the raw data, but not effectively improve results. The results presented here are therefore obtained from raw data, without preprocessing.

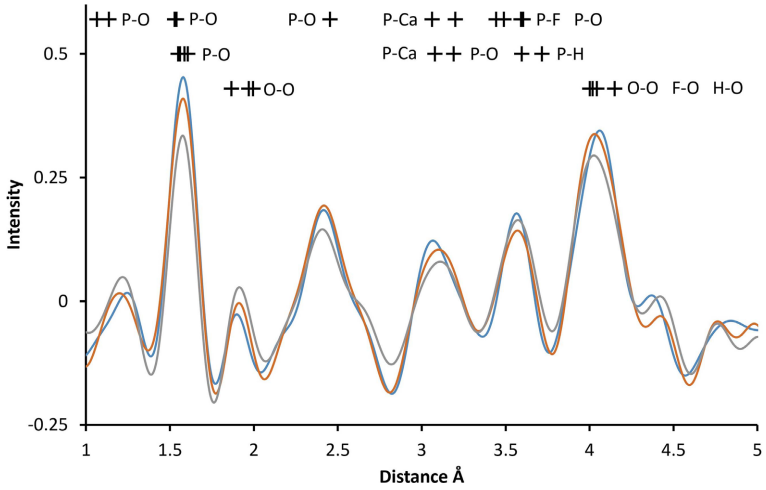

Figure 6. Distribution of interatomic distances for K31, K32, and K33 samples. Blue line: K31; red line: K32; brown line: K33.

In **Figure 7**, the simulation of the structures was performed using the PDFfit software. Generally, the parameters that can be calculated with PDFfit are the scale, the instrument resolution, and the structural parameters, namely the width of the first peak due to correlated motion (δ), the lattice parameters, and the atomic positions. However, the occupancy factors cannot be effectively refined in such complex mineral mixtures. To refine the model, we assigned the same displacement parameter to the different types of atoms. Finally, the atomic positions of the calcium, phosphorus, silicon, and oxygen atoms were calculated. In general, the method yielded a relatively stable solution that was consistent with the Pair Distribution Functions (PDFs).

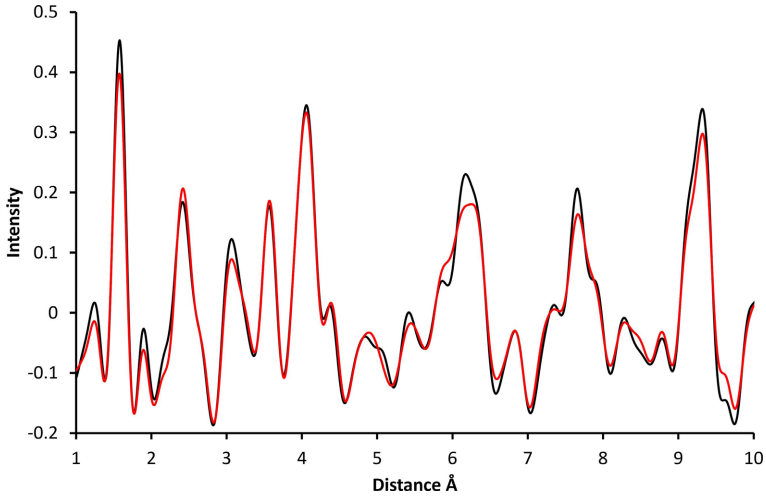

Figure 7. Pdffit of the K31 phosphorite. Black line: experimental data; red line: simulation. The K31 pattern is very similar to K32 and K33 patterns.

4. Discussion

The rocks of Kotchari deposits consist of different phosphorite types associated

with siliceous minerals. X-ray diffraction (XRD) analysis of the rocks has shown the coexistence of apatite group minerals, mainly hydroxyapatite and francolite [28].

Francolite (Ca, Mg, Sr, Na)10(PO_4, SO_4, CO_3)6F_{2-3} is a carbonate-rich fluorapatite with frequent Ca, PO_4, and F substitutions at all sites [29]. It occurs within phosphorite layers and is primarily associated with hydroxyapatite. The relative abundance of francolite depends on the type of geological processes, their duration, and the nature of the local environment [30].

The coexistence of hydroxyapatite and francolite has already been recognized in numerous studies on phosphate rock deposits. It has been shown that hydroxyapatite was initially formed by a natural process, particularly in marine environments. This mineral gradually transforms into francolite through recrystallization and diffusion processes. This is accompanied by structural substitutions of PO_4 groups by CO_2 and F, and it has been shown that the rate of substitutions is correlated with the degree of crystallinity of francolite.

In **Table 3**, the chemical compositions are reported with Standard Deviations (SD). It evidences that XRF is the most accurate method, but Rietveld simulation provides a satisfying evaluation of the chemical compositions.

Values obtained by XRF indicate that calcium oxide (CaO), phosphorus pentoxide (P_2O_5), and silicon dioxide (SiO_2) are the major oxides. Their contents are correlated with the industrial use of these rocks, and the CaO/P_2O_5 weight ratio is a common criterion for deposit quality. For samples K31, K32, and K33, and from Rietveld simulation, the ratio is close to the average of 1.34, which is below the value of 1.58 for pure francolite and hydroxylapatite. From XRF, the values are more widely distributed, from 1.27, 1.34, and 1.42. The discrepancy is from the difference in Standard Deviations in **Table 3**.

This relative decrease in CaO content is due to the presence of silica and minor minerals, such as illite. By comparison, most commercially available phosphates have a CaO/P_2O_5 ratio of up to 1.6.

Table 3 also compares XRF analyses with oxide quantities calculated by quantitative Rietveld simulation, considering the chemical compositions of the identified minerals. The small differences in chemical element content highlight the accuracy of the results, confirming the effectiveness of the Rietveld method. However, the method's limitations also depend on the detection threshold, which is determined by the mineral type and its degree of crystallinity. For phosphate-type minerals, the calculated oxide contents are close to those obtained by XRF. In general, while a slight discrepancy appears for all oxides, it is less pronounced for the major oxides SiO_2, CaO, and P_2O_5. Nevertheless, the exact stoichiometry of the mineral phases is poorly known, especially for carbonate-fluorapatite (francolite) and hydroxylapatite. Information on structural characteristics of the mineral phases used in the Rietveld simulations is in **Table 4**. Grain sizes are also reported (nm), in the (111) direction. Whereas phases exhibit deviations from ideality, a more precise simulation could only be obtained after a separation method of minerals.

Table 3. Chemical composition and standard deviations of K31, K32, and K33 phosphorites, obtained by XRF and calculated from the mineralogical analyses from the Rietveld method.

	Calculated (%)			SD (%)	XRF (%)			SD (%)
	K31	K32	K33		K31	K32	K33	
H_2O	0.61	0.77	0.68	0.1	0.58	0.75	0.66	0.05
CO_2	0.21	0.23	0.23	0.1	0.22	0.21	0.24	0.05
F	0.99	1.06	1.08	0.1	0.92	1.01	1.02	0.05
Al_2O_3	2.36	1.13	1.83	0.3	2.49	1.02	1.88	0.1
SiO_2	31.25	21.92	25.32	0.5	31.37	20.48	24.96	0.2
P_2O_5	27.14	31.82	29.93	0.5	27.98	33.69	29.01	0.2
K_2O	1.09	0.52	0.85	0.1	1.03	0.52	0.88	0.05
CaO	36.35	42.55	40.08	0.5	35.43	42.32	41.36	0.2

Table 4. Structural characteristics of the mineral phases used in the Rietveld simulations. All dimensions are in nm, and the grain sizes are in the (111) direction.

ID		K31	K32	K33
Quartz	a	0.491405	0.491403	0.491373
	c	0.54055	0.54056	0.540495
	Size	366	320	445
Hydroxylapatite	a	0.93647	0.93661	0.93667
	c	0.6898	0.68965	0.68981
	Size	70.1	67.2	64
Francolite	a	0.93496	0.935	0.93512
	c	0.68899	0.68888	0.6889
	Size	91	86	83
Illite	a	0.515008	0.5227	0.515008
	b	0.88899	0.88899	0.88899
	c	1.01237	1.01237	1.03283
	beta	100.554	100.554	102.586
	Size	3	5	3

Regarding the contents of minor oxides (Na_2O, K_2O, MgO, and Fe_2O_3), the detection limit of XRD is a limitation observed in these samples, and the relative accuracy of the contents is lower. One source of discrepancy is due to the ion distribution in the structures of the different minor minerals, with possible substitutions in the crystal lattices. The discrepancy is also related to the amount of fluorine, which, according to the results obtained, originates only from francolite. This is observed despite the unlikely possibility of over stoichiometry, since the composition of this mineral is relatively constant in different phosphorites. This re-

sults from the formation process of francolites in solutions of relatively constant composition, *i.e.*, in seawater [30].

For the Kotchari deposit, the Fluor content obtained by XRF is higher than that which was analyzed by Rietveld simulation, and no other mineral than francolite was identified in the compositions. To attain a higher fluorine content through simulation, it should be noted that the Rietveld method with a mixture of different apatite group minerals and non-phosphate minerals cannot lead to an ideal solution when widely varying the substitution rates of PO_4 by CO_3 and F. This is due to difficulties related to the convergence of calculations with phases having strong structural similarities, which is the case for hydroxyapatite and francolite.

Iron analyzed by XRF is also not systematically detected by Rietveld simulations when it does not originate from iron minerals. However, iron is frequently analyzed by XRF in phosphorites, as it plays a major role in the precipitation of francolite in many organic-poor environments [30]. In our samples, this is mainly due to the low iron content and the absence of iron minerals. Most of the iron is very likely substituted for aluminum in the major minerals and also in illite. It is also possible that a small amount of iron hydroxide is present, but below the detection threshold of the X-ray diffraction method.

Information on the structural characteristics of the mineral phases is also provided by the interpretation of the Pair Distribution Function (PDF) curves in **Figure 6**. These curves allow the identification of the most frequent interatomic distances in the predominant mineral phases. According to **Figure 6**, only small differences in peak intensity values are observed on the curves for rocks K31, K32, and K33. In particular, peaks related to P-O bond groups are distinguished at approximately 1.21 - 1.27 Å, 1.58 - 1.59 Å, and 2.42 - 2.43 Å. P- Ca and P-O bonds are also identified around 3.07 - 3.1 Å and P-F and P-H bonds near 3.53 - 3.56 Å. Finally, F-O and H-O bonds are identified around 4.03 - 4.06 Å. It is seen that the interatomic distances in hydroxylapatite and francolite are very similar (**Figure 6**), and the simulation of the spectra gives results almost identical to those shown in **Figure 7**.

The structure of francolite reveals the presence of F-P and F-O bonds. However, the PDF characteristics do not allow for the identification of Ca-F bonds at 2.3059 Å and 4.41277 Å, and Ca-Ca bonds at 3.76322 Å, which could be found in structures of various fluorine minerals such as CaF_2. This confirms the low probability of identifying fluorine-containing minerals, other than francolite, above a detectable concentration.

5. Conclusions

The work showed that the detection threshold of iron and fluorine is equivalent to their concentration in fluorites. Despite this, the studies demonstrated that Rietveld simulations of high-resolution X-ray diffraction patterns reliably determine the mineralogical composition of phosphorites, although they are complex mineralogical compositions. This result is validated by a correlation between the

chemical composition values calculated from the mineralogical compositions of the identified minerals and the chemical composition values obtained by XRF.

It was also shown that the characterization of phosphorites is particularly complex due to the coexistence of at least two mineral phases from the apatite group. Similarly, this phenomenon has also been identified in the study of different African phosphorite deposits. In the case of the Kotchari deposit, the coexistence of the hydroxylapatite and francolite mineral phases is clearly demonstrated by the detailed identification of X-ray diffraction patterns and by Rietveld simulations. In all cases, the accuracy of the phase identification and simulations is significantly improved by the specific characteristics of the high-resolution X-ray diffraction patterns from the ESRF synchrotron.

Despite the strong similarity in the structural characteristics of hydroxylapatite and francolite, it is possible to accurately calculate the mineral phase contents. This is obtained accurately, although it was necessary to limit the variations of lattice parameters and the substitution rates of PO_4 groups by CO_3 and F, and also of Al by Fe.

The identification of mineral phases correlates well with the interpretation of Atomic Pair Distribution (APD) curves. Simulation of these curves allowed for the identification of the predominant interatomic bonds in the structures of hydroxylapatite and francolite. Simultaneously, the APD curves did not reveal the presence of F-P and F-Ca bonds, indicating that excess fluorine and iron relative to the ideal mineral stoichiometry are distributed within the rock's mineral structures.

The obtained mineralogical compositions are very satisfactory, although the contents of minor elements that are structurally substituted, such as fluorine and iron, are slightly underestimated. The used method allows to very rapidly perform hundreds of experiments at a reduced cost. Rietveld simulations can be achieved semi automatically, reducing the computational cost. The research opens up perspectives for improving the management of mineral deposits.

Acknowledgements

The authors gratefully acknowledge the long-term support of the research institutions that made the study possible. They are the Laboratory of Molecular Chemistry and Materials (LC2M), Joseph KI-ZERBO University in Ouagadougou, the Laboratory of Geoscience and Environmental Science (LaGE), Joseph KI-ZERBO University in Ouagadougou, and the Laboratory IRCER in Limoges University, France.

We also acknowledge the European Synchrotron Radiation Facility (ESRF) for the provision of synchrotron radiation facilities and Momentum Transfer for facilitating the measurements. Jakub Drnec is thanked for assistance and support in using beamline ID31. The measurement setup was developed with funding from the European Union's Horizon 2020 research and innovation program under the STREAMLINE project (grant agreement ID 870313). OSCARS supported meas-

urements performed as part of the MatScatNet project through the European Commission's Horizon Europe Research and Innovation program under the grant agreement No. 101129751.

Author Contributions

Methodology, Jean Baptiste Zoungrana; resources, writing—review and editing, Brahima Sorgho; methodology, Lamine Zerbo; methodology, Gisèle Lecomte Nana; software—writing—review and editing, Philippe Blanchart. All authors have read and agreed to the published version of the manuscript.

Conflicts of Interest

The authors declare no conflicts of interest regarding the publication of this paper.

References

[1] Sánchez, F. and Hartlieb, P. (2020) Innovation in the Mining Industry: Technological Trends and a Case Study of the Challenges of Disruptive Innovation. *Mining, Metallurgy & Exploration*, **37**, 1385-1399. https://doi.org/10.1007/s42461-020-00262-1

[2] Maksarov, V.V., Gabov, V.V., Zadkov, D. and Martyushev, N.V. (2020) Mining Industry: Innovations and Prospects for the Development of Materials Science. Trans Tech Publications Ltd.

[3] Ali, A., Chiang, Y.W. and Santos, R.M. (2022) X-Ray Diffraction Techniques for Mineral Characterization: A Review for Engineers of the Fundamentals, Applications, and Research Directions. *Minerals*, **12**, Article 205. https://doi.org/10.3390/min12020205

[4] Santini, T.C. (2015) Application of the Rietveld Refinement Method for Quantification of Mineral Concentrations in Bauxite Residues (Alumina Refining Tailings). *International Journal of Mineral Processing*, **139**, 1-10. https://doi.org/10.1016/j.minpro.2015.04.004

[5] Coelho, A.A. (2018) Topas and Topas-Academic: An Optimization Program Integrating Computer Algebra and Crystallographic Objects Written in C++. *Journal of Applied Crystallography*, **51**, 210-218. https://doi.org/10.1107/s1600576718000183

[6] Peng, Q.M., Wang, Z.Z., Wang, G.W., Zhang, W.G., *et al.* (2023) 3D Mineral Prospectivity Mapping from 3D Geological Models Using Return—Risk Analysis and Machine Learning on Imbalance Data. *Minerals*, **13**, Article 1384. https://doi.org/10.3390/min13111384

[7] Zhang, Z.Q., Wang, G.W., Carranza, E.J.M., Li, W., Li, Y., Tang, L., *et al.* (2025) Three-Dimensional Mineral Prospectivity Mapping Using a Residual Convolutional Neural Network with Lightweight Attention Mechanisms. *Ore Geology Reviews*, **185**, Article 106797. https://doi.org/10.1016/j.oregeorev.2025.106797

[8] Wang, J.L., Mao, X.C., Liu, Z.K., Deng, H., *et al.* (2024) Three-Dimensional Mineral Prospectivity Mapping Considering Structural Restoration in the Dayingezhuang Gold Deposit, Eastern China. *Ore Geology Reviews*, **165**, Article 105860. https://doi.org/10.1016/j.oregeorev.2023.105860

[9] Taylor, M., Wall, J., Loxley, N., Wormington, M. and Lafford, T. (2001) High Resolution X-Ray Diffraction Using a High Brilliance Source, with Rapid Data Analysis by Auto-Fitting. *Materials Science and Engineering: B*, **80**, 95-98. https://doi.org/10.1016/s0921-5107(00)00621-8

[10] Gualtieri, A.F., Gatta, G.D., Arletti, R., Artioli, G., Ballirano, P., Cruciani, G., Guagliardi, A. and Malferrari, D. (2019) Quantitative Phase Analysis Using the Rietveld Method: Towards a Procedure for Checking the Reliability and Quality of the Results. *Periodico di Mineralogia*, **88**, 147-151.

[11] Doebelin, N. and Kleeberg, R. (2015) Profex: A Graphical User Interface for the Rietveld Refinement Program BGMN. *Journal of Applied Crystallography*, **48**, 1573-1580. https://doi.org/10.1107/s1600576715014685

[12] Gražulis, S., Daškevič, A., Merkys, A., Chateigner, D., Lutterotti, L., Quirós, M., *et al.* (2012) Crystallography Open Database (COD): An Open-Access Collection of Crystal Structures and Platform for World-Wide Collaboration. *Nucleic Acids Research*, **40**, D420-D427. https://doi.org/10.1093/nar/gkr900

[13] Bonitz, M., Hennig, T., Schleicher, A.M., Jaeggi, D., Stammeier, J.A., Ostertag-Henning, C., *et al.* (2025) Bulk Rock Geochemical and Mineralogical Characterisation of Clay-Rich Sediments from Drill Core Analysis of the Staffelegg Formation. *Applied Geochemistry*, **186**, Article 106389. https://doi.org/10.1016/j.apgeochem.2025.106389

[14] Haračić, N., Jovanovic, M., Merdić, N. and Mujkanović, A. (2025) Evaluation of Profex Software for Phase Analysis of Cement, Clinker, and Limestone: A Comparative Study with Topas. 15*th Scientific/Research Symposium on Metallic and Non-Metallic Materials*, Zenica, 24-25 April 2025, 1-11. https://mnm.unze.ba/article/278/pdf

[15] Billinge, S.J.L. and Kanatzidis, M.G. (2004) Beyond Crystallography: The Study of Disorder, Nanocrystallinity and Crystallographically Challenged Materials with Pair Distribution Functions. *Chemical Communications*, **7**, 749-760. https://doi.org/10.1039/b309577k

[16] Proffen, T., Page, K.L., McLain, S.E., Clausen, B., Darling, T.W., TenCate, J.A., *et al.* (2005) Atomic Pair Distribution Function Analysis of Materials Containing Crystalline and Amorphous Phases. *Zeitschrift für Kristallographie—Crystalline Materials*, **220**, 1002-1008. https://doi.org/10.1524/zkri.2005.220.12.1002

[17] European Synchrotron Radiation Facility. 38043 Grenoble France. https://www.esrf.fr/home/UsersAndScience/Applying.html

[18] https://www.esrf.fr/home/news/tech-talk/content-news/tech-talk/techtalk13.html

[19] Lucas, J., Prévôt, I.L. and Trompette, R. (1980) Petrology, Mineralogy and Geochemistry of the Late Precambrian Phosphate Deposits of Upper Volta (W Africa). *Journal of the Geological Society*, **137**, 787-792. https://doi.org/10.1144/gsjgs.137.6.0787

[20] Zoungrana, J.B., Sorgho, B., Bakouan, C., Sawadogo, S., Ouedraogo, R.D., Guel, B., *et al.* (2024) Mineralogical Study of Phosphate Rocks by Quantitative Rietveld Refinement. *Open Ceramics*, **18**, Article 100567. https://doi.org/10.1016/j.oceram.2024.100567

[21] Terban, M.W. and Billinge, S.J.L. (2021) Structural Analysis of Molecular Materials Using the Pair Distribution Function. *Chemical Reviews*, **122**, 1208-1272. https://doi.org/10.1021/acs.chemrev.1c00237

[22] Egami, T. and Billinge, S.J.L. (2003) Underneath the Bragg Peaks: Structural Analysis of Complex Materials. *Materials Today*, **6**, 57. https://doi.org/10.1016/s1369-7021(03)00635-7

[23] Billinge, S. and Jensen, K. (2023) Atomic Pair Distribution Function Analysis: A Primer. International Union of Crystallography Texts on Crystallography. Oxford University Press.

https://global.oup.com/academic/product/atomic-pair-distribution-function-analysis-9780198885801?cc=fr&lang=en&

[24] Juhás, P., Davis, T., Farrow, C.L. and Billinge, S.J.L. (2013) PDFgetX3: A Rapid and Highly Automatable Program for Processing Powder Diffraction Data into Total Scattering Pair Distribution Functions. *Journal of Applied Crystallography*, **46**, 560-566. https://doi.org/10.1107/s0021889813005190

[25] Farrow, C.L., Juhas, P., Liu, J.W., Bryndin, D., Božin, E.S., Bloch, J., *et al.* (2007) PDFfit2 and PDFgui: Computer Programs for Studying Nanostructure in Crystals. *Journal of Physics*: *Condensed Matter*, **19**, Article 335219. https://doi.org/10.1088/0953-8984/19/33/335219

[26] Billinge, S.J.L. and Farrow, C.L. (2013) Towards a Robust Ad Hoc Data Correction Approach That Yields Reliable Atomic Pair Distribution Functions from Powder Diffraction Data. *Journal of Physics*: *Condensed Matter*, **25**, Article 454202. https://doi.org/10.1088/0953-8984/25/45/454202

[27] Altomare, A., Corriero, N., Cuocci, C., Falcicchio, A., Moliterni, A. and Rizzi, R. (2015) QUALX2.0: A Qualitative Phase Analysis Software Using the Freely Available Database POW_COD. *Journal of Applied Crystallography*, **48**, 598-603. https://doi.org/10.1107/s1600576715002319

[28] Boulemia, S., Hadji, R., Bouhlal, S., Hamed, Y., Besser, H. and Ncibi, K. (2023) Geological and Mineralogical Analysis of Phosphorites in the Jebel Dhyr Syncline, Eastern Algerian Atlas. *Mineralogia*, **54**, 89-104. https://doi.org/10.2478/mipo-2023-0010

[29] Jarvis, I., Burnett, W.C., Nathan, Y., Almbaydin, F.S.M., *et al.* (1994) Phosphorite Geochemistry State-of-the-Art and Environmental Concerns. *Eclogae Geologicae Helvetiae*, **87**, 643-700. https://hero.epa.gov/reference/4842433/

[30] Mcarthur, J.M. (1985) Francolite Geochemistry—Compositional Controls during Formation, Diagenesis, Metamorphism and Weathering. *Geochimica et Cosmochimica Acta*, **49**, 23-35. https://doi.org/10.1016/0016-7037(85)90188-7